Journal of Power Sources xxx (xxxx) xxx

Contents lists available at ScienceDirect

Journal of Power Sources

journal homepage: www.elsevier.com/locate/jpowsour

Energy transfer for storage or recovery in capacitive deionization using a DC-DC converter

Diego I. Oyarzun [a,b], Steve A. Hawks [b], Patrick G. Campbell [b], Ali Hemmatifar [c], Ashish Krishna [a], Juan G. Santiago [a,*], Michael Stadermann [b,**]

[a] Department of Mechanical Engineering, Stanford University, Stanford, CA, 94305, USA
[b] Lawrence Livermore National Laboratory, Livermore, CA, 94550, USA
[c] Department of Chemical Engineering, Massachusetts Institute of Technology, Cambridge, MA, 02139, USA

HIGHLIGHTS

- Proposed energy transfer efficiency metrics from (one-way) and to (round-trip) CDI.
- Presented a model to predict energy transfer between a CDI cell and a supercapacitor.
- Energy transfer efficiency of CDI-to-SC can be ~90% for reasonable system parameters.

ARTICLE INFO

Keywords:
Capacitive deionization
Energy recovery efficiency
Buck-boost converter
Energy transfer
Supercapacitor

ABSTRACT

Energy recovery from capacitive deionization (CDI) has the potential to increase overall desalination efficiency. We here define the storage (one-way) and utilization (round-trip) efficiencies between a CDI cell and an energy storage device using a generic direct current/direct current (DC/DC) converter circuit. Presented is a closed-form analytical model for the case of a supercapacitor (SC) as the energy storage device and a buck-boost converter as the DC/DC converter. The model is benchmarked with a numerical model, showing good agreement. Also presented is a comparison among energy transfer methods wherein desalination productivity is fixed. For constant current operation, this condition requires higher currents to compensate for the inactive time introduced by the converter. For fixed productivity, the mean current of the converter circuit approaches the constant current value for higher initial voltages and lower capacitances in the supercapacitor. Finally, we show the effect of relevant parameters of the SC in the storage and utilization efficiency. The model predicts storage and utilization efficiencies of at least 90% for an initial voltage of 1 V or higher and reasonable CDI and SC parameters. Lastly, we provide engineering operational parameters to maximize the efficiency of energy transfer and guidance in the selection of electronic components.

1. Introduction

Water [1,2] and energy [2] scarcity is a global concern. There has been a growth in interest over the last decade for methods for treatment of moderate and low ionic strength solutions, such as brackish water [3–6]. Capacitive deionization (CDI) provides an interesting alternative and energy efficient [7–9] technique for desalination of relatively low salinity (e.g. brackish) water streams [10–13] and for selective removal of contaminants [14–21]. Unlike reverse osmosis or thermal desalination, CDI does not require high pressure or temperature [10,11], and the primary energy input of CDI is electric power at low voltage [22,23].

A typical CDI architecture consists of at least one pair of activated carbon porous electrodes. Under an externally applied electric field, ionic species are trapped within electric double layers inside pores [23]. The applied bias (during the adsorption step) can be supplied at constant current [24–26], constant voltage [24–26], or arbitrary functions of either current or voltage [27]. After some adsorption, the CDI cell is discharged creating a high salinity brine solution. Interestingly, by far the most common discharge method to date for CDI is simply short circuit (0 V) [10,11,22,23,28–32]. Such discharge offers no opportunity to recover or reuse energy.

* Corresponding author.
** Corresponding author.
E-mail addresses: juan.santiago@stanford.edu (J.G. Santiago), stadermann2@llnl.gov (M. Stadermann).

https://doi.org/10.1016/j.jpowsour.2019.227409
Received 25 July 2019; Received in revised form 31 October 2019; Accepted 4 November 2019

Nomenclature

C_{CDI}	Effective capacitance of the CDI cell
C_{SC}	Capacitance of the supercapacitor
$E_{CDI,rec}$	Energy recovered into the CDI cell from the energy storage (ES) device
$E_{ES,sto}$	Energy stored into the ES from the CDI cell
$E_{in,CDI}$	Energy input into the CDI
$E_{in,ES}$	Energy input into the ES
$E_{L,CDI,ch}$	Energy lost (e.g. to heat) within the CDI cell during charge
$E_{L,CDI,dis}$	Energy lost in the CDI cell during discharge
$E_{L,DC-DC}$	Energy lost in the DC-DC converter
$E_{L,SC,ch}$	Energy lost in the SC during charge
$E_{L,SC,dis}$	Energy lost in the SC during discharge
$E_{out,CDI}$	Energy output from the CDI
$E_{out,ES}$	Energy output from the SC
$E_{\$}$	External energy input (top-off) required to drive a desalination cycle ($E_{\$}$ is equal to the summation of all energy lost in the cycle)
I_1	Maximum CDI output (input) current which triggers buck-boost switch during discharge (charge) of CDI
I_2	Maximum SC input (output) current which triggers buck-boost switch during charge (discharge) of SC
ΔI	Current window defined as $(I_2 - I_1)$
I_{cc}	Constant current value representing typical research-type operation using a sourcemeter
I_{mean}	Mean current for buck-boost operation, defined as the arithmetic mean of I_1 and I_2
$I_{mean,P}$	Mean current for buck-boost operation and for fixed productivity
I_{RMS}	Root mean square (RMS) current used to calculate energy losses for a triangular current profile
$I_{RMS,P}$	RMS for condition of fixed productivity
L	Inductance of inductor
q_{CDI}	Change of electrical charge in the CDI cell
q_{SC}	Change of electrical charge in the SC
$R_{eq,CDI}$	Sum of series resistance of the CDI cell and inductor resistance
$R_{eq,SC}$	Sum of series resistance of the SC with the inductor resistance
R_{CDI}	Series resistance of the CDI cell
R_{ES}	Series resistance of the energy storage component
R_L	Series resistance associated with the inductor
R_{SC}	Effective series resistance of the supercapacitor
$t_{cc,dis}$	Total time to discharge a CDI cell at constant current I_{cc}
$t_{dis,total}$	Total time to discharge a CDI cell as the addition of $t_{off,dis}$ with $t_{on,dis}$
$t_{off,dis}$	Total time spent actively charging to or from the SC (CDI inactive time) during the discharge of a CDI cell
$t_{on,dis}$	Total time spent actively charging to or from the CDI cell (CDI active time) during discharge of CDI
$\Delta t_{off,dis}$	Time spent in an individual buck-boost cycle in the SC during discharge of the CDI cell
$\Delta t_{on,dis}$	Time spent in an individual buck-boost cycle in the CDI cell during discharge of the CDI cell
$V_{CDI,i}$	Initial voltage of the CDI cell
$V_{CDI,f}$	Final voltage of the CDI cell
$V_{SC,i}$	Initial voltage of the SC
$V_{SC,f}$	Final voltage of the SC
η_{util}	Utilization (round-trip) efficiency
$\eta_{util+CDI}$	Overall system efficiency for utilization (round-trip) and desalination
η_{sto}	Storage (one-way) efficiency
$\eta_{sto+CDI}$	Overall system efficiency for storage (one-way) and desalination

Over the last decade, several groups have employed various DC/DC converters to harvest electricity from low power applications, including solar cells [33,34], thermoelectric generators [35], and fuel cells [36,37]. CDI is an ideal candidate for energy recovery with a DC/DC converter, as the stored energy in the electric double layers (analogous to an electrolytic supercapacitor, SC) can be transferred into a storage device (or another CDI cell). For CDI, energy harvesting is an opportunity to increase the overall desalination efficiency. There have been several efforts towards efficient energy transfer from CDI cells [38–47]. The type and values of figures of merit related to energy transfer vary widely among these studies. For instance, Kang et al. [38] showed energy transfer from an MCDI cell to a supercapacitor (and not vice versa) with a buck-boost converter and defined energy transfer efficiency as the recovered energy into a supercapacitor over the total energy input into the membrane capacitive deionization (MCDI) cell. The reported energy recovery efficiency ranged from less than 5% to up to 45%. A study published by Alkuran et al. [41] reported measurements for energy transfer between an electrical circuit designed to emulate a CDI cell and a supercapacitor using a buck-boost converter. Alkuran et al. [41] defined energy efficiency as the energy stored into the SC (starting at 0 V) divided by the total energy input into the capacitor of the CDI cell circuit. The reported efficiencies varied from 51% to 64%. Pernia et al. [39,40] considered the transfer of energy to an SC using an electrical circuit to emulate a CDI cell and showed efficiencies of up to 84% [39] and 89% [40]. To date, there are no systematic definitions of figures of merit for CDI energy transfer. Also, models have to date provided no direct analytical relations useful in the identification of key parameters. Further, to our knowledge, there have been no studies of the energetics associated with the transfer of energy from the CDI cell to a storage device and then the transfer of energy back to the CDI cell (i.e., no "round-trip" type studies).

We here consider two scenarios of CDI energy transfer. First, the energy is transferred from the CDI cell to the storage—a one-way transfer of energy. Second, the energy is transferred from the cell to the storage and then the energy is transferred back from the storage to the cell. We define clear figures of merit for a generic DC/DC converter for each scenario and compare and contrast these with existing similar figures of merit. To model the system, we chose a buck-boost converter to transfer energy and a supercapacitor (SC) for the storage method. We first present a computer simulation which models dynamics of the buck-boost converter dynamics in a piecewise manner leveraging solutions to ordinary differential equations (ODE) for each charging step. Next, we develop and propose an analytical model which is benchmarked with the piecewise-ODE simulations. This analytical model is advantageous in identifying key parameters and in design and control efforts to predict energy losses, storage efficiency, and utilization efficiency. Finally, we show the effect of circuit and control parameters to the figures of merit we propose. These provide insight into the selection of electronic components and key operational parameters required to maximize the energy transfer efficiencies.

2. Energy transfer efficiency for storage (one-way) or utilization (round-trip)

DC/DC converters offer a convenient method of recovering energy from CDI systems. For low power applications, some of the available

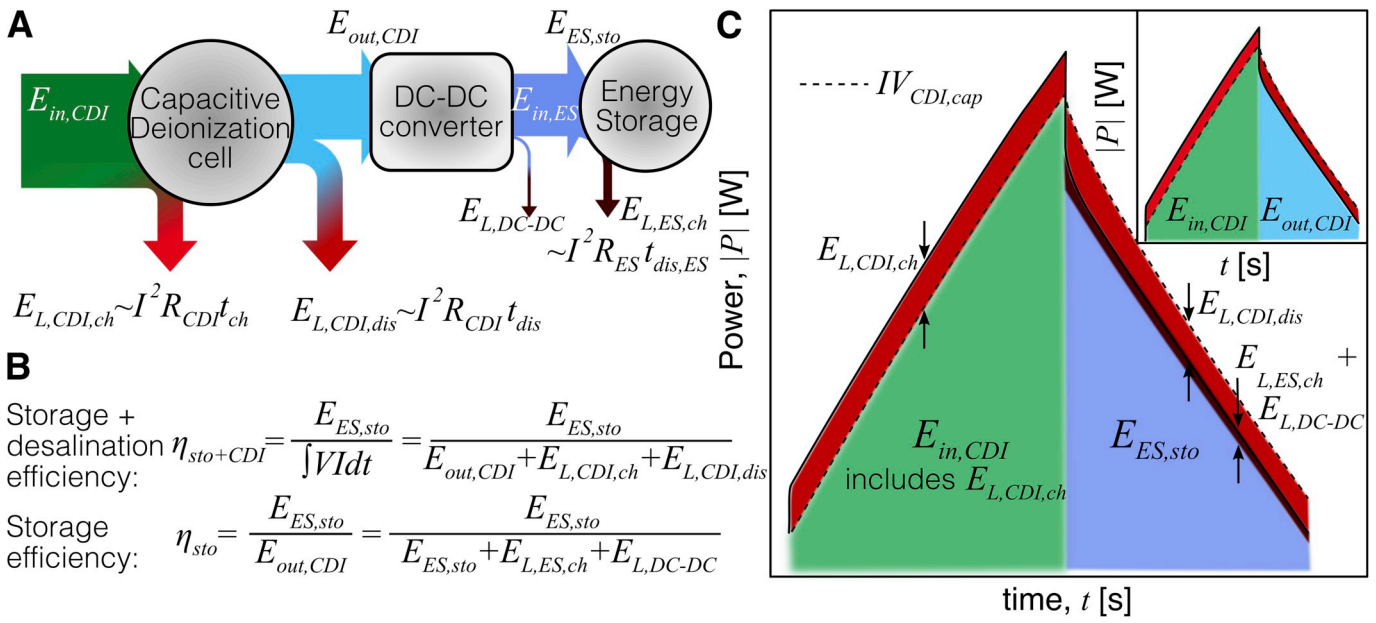

Fig. 1. (**A**) Schematic of the on-way energy transfer (i.e. energy storage) with a generic DC-DC converter from a CDI cell to an energy storage (ES) device. Labels $E_{in,CDI}$, $E_{out,CDI}$, and $E_{in,ES}$ correspond to the total energy into the CDI cell, out the CDI cell, and into the ES respectively. $E_{ES,sto}$ is the effective energy stored into the ES. The red arrows represent energy losses, $E_{L,j}$, from each component *j*. (**B**) Definition of the recovery efficiency that includes CDI performance $\eta_{sto+CDI}$ and the current proposed definition which accounts for only the storage efficiency η_{sto}. (**C**) Schematic of a standard power consumption curve of a CDI cell operated at constant current (charge and discharge) with energy recovery. Shaded areas are labeled as in Fig. 1A. Inset shows the schematic of a CDI cell at constant current operation without energy recovery. (For interpretation of the references to colour in this figure legend, the reader is referred to the Web version of this article.)

configurations are boost [48], Ćuk [48,49], buck-boost [49], or SEPIC [49,50] converters. The choice of the converter depends on the current/voltage characteristics of the system and the final use of the energy. For example, there are two categories [51] in photovoltaic systems: stand-alone and grid-connected application. The former is used for energy storage, while in the latter energy is directly consumed. In CDI, the

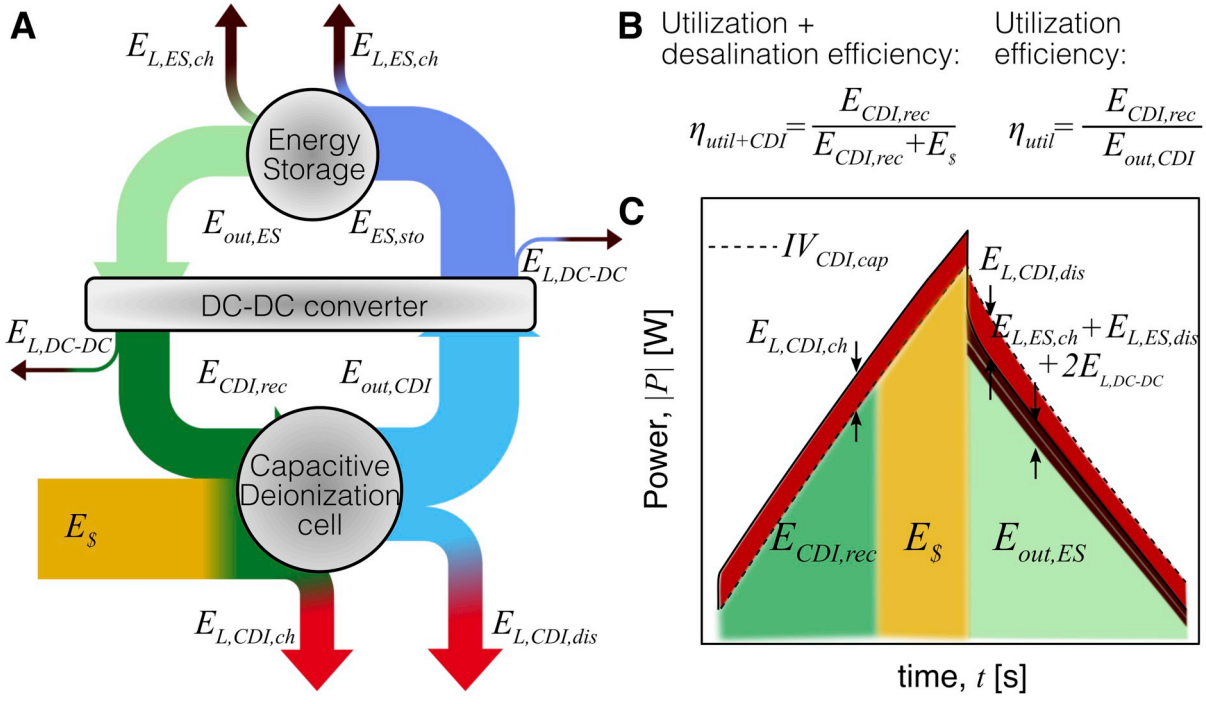

Fig. 2. (**A**) Schematic of the full cycle of energy transfer with a generic DC-DC converter from a CDI cell to an energy storage device, ES. $E_{\$}$ is the extra energy that should be supplied to the cycle during the charge of the CDI cell. $E_{in,CDI}$, $E_{out,CDI}$, $E_{in,ES}$, and $E_{out,ES}$ correspond to the total energy into the CDI cell, out of the CDI cell, into the ES, and out of the ES, respectively. $E_{CDI,rec}$ is the recovered (or utilized) energy from the storage device. $E_{ES,sto}$ is the energy stored in the ES device. The red arrows represent energy losses, $E_{L,j}$, at each *j* component. (**B**) Definition of the recovery efficiency that includes CDI performance $\eta_{util+CDI}$ and our proposed definition that only accounts for the utilization efficiency η_{util}. (**C**) Schematic of a standard power consumption curve at constant current of a CDI cell (charge and discharge) with energy recovery. Shaded areas are labeled as in Fig. 2A. (For interpretation of the references to colour in this figure legend, the reader is referred to the Web version of this article.)

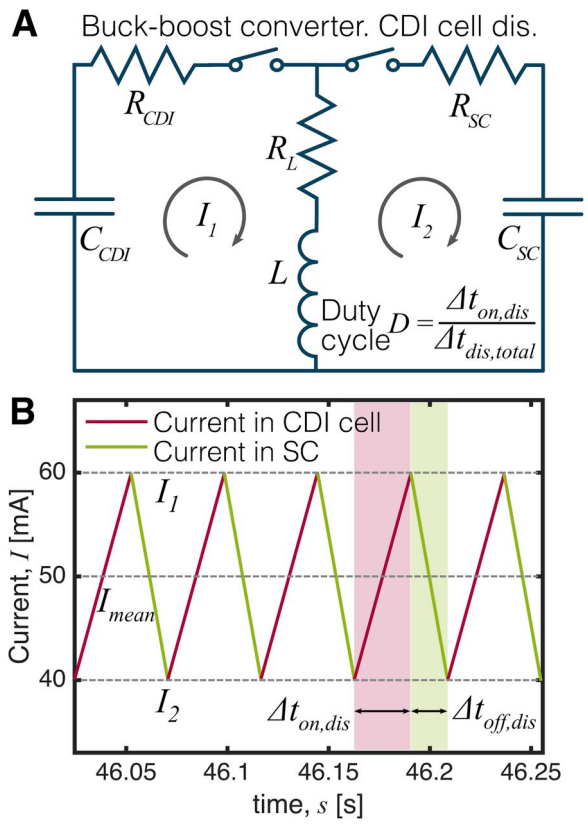

Fig. 3. (**A**) Schematic of the simplified circuit of a buck-boost converter for energy transfer between a CDI cell and an SC during the discharge of the CDI cell. (**B**) ODE model predictions of current versus time for typical parameters for energy transfer with a buck-boost converter. I_1 and I_2 represent the upper and lower current limits. The current window is given by I_1 - I_2 or ΔI. The time at positive slopes in the schematic corresponds to the active time, $\Delta t_{on,dis}$, while the time at negative slopes to the inactive time, $\Delta t_{off,dis}$, during discharge. Fixed parameters used in this figure are as follows: $C_{CDI} = C_{SC} = 10$ F, $V_{CDI,i} = 1$ V, $V_{CDI,f} = 0.4$ V, $V_{SC,i} = -1$ V, $\Delta I = 20$ mA, $R_{CDI} = 3\ \Omega$, $R_{SC} = 0.1\ \Omega$ and $R_L = 0.01\ \Omega$.

purpose of the DC/DC converter can be either storage or utilization of the electrical power in the next desalination cycle. Therefore, a bi-directional converter (such as the buck-boost converter) is an attractive option for energy recovery in CDI. In this section, we provide a framework for energy recovery efficiencies that applies to any DC/DC converter. We recognize and present two possible energy recovery schemes, a one-way energy transfer for energy storage and a round-trip for energy utilization in the CDI cell.

2.1. Energy transfer for storage (one-way) in CDI using a generic DC/DC converter

Fig. 1A shows the schematic of a system consisting of a CDI cell connected to a DC/DC converter. The generic converter is connected to a (generic) electrical energy storage (ES) device. In Fig. 1A, the arrows represent the total energy into or out of the components of the cycle due to an energy flux across the boundaries of the CDI cell, DC/DC converter, and the ES device. $E_{in,CDI}$, $E_{out,CDI}$, and $E_{in,ES}$ are respectively the total energy into the CDI cell, out of the CDI cell, and into the ES. Further, $E_{ES,sto}$ is the energy stored into the energy storage device. $E_{ES,sto}$ is calculated as the subtraction between $E_{in,ES}$ and the energy lost $E_{L,ES,ch}$ during the charge of the ES. The red arrows represent energy losses from the system (e.g., due to heat).

Fig. 1B shows a comparison between the proposed metric for energy storage efficiency η_{sto} and a standard definition of energy transfer efficiency (i.e., storage plus desalination efficiency, $\eta_{sto+CDI}$). The latter definition is a quantification of the overall system efficiency, which combines desalination and energy recovery efficiency. Note that overall system efficiency includes the energy losses associated with and inherent to simply operating the CDI desalination process, irrespective of whether energy is transferred in or out using a DC/DC converter. Although the overall system efficiency is a global indicator of the performance of the system, $\eta_{sto+CDI}$ is not applicable to the reporting of the volumetric desalination energy. Hawks et al. [52] defined volumetric desalination energy consumption as $E_v = (E_{in} - \eta E_{out})/V_d$. Here, V_d is the volume of desalinated water, E_{in} is the total energy input into the CDI cell (analogous to $E_{in,CDI}$ in Fig. 1A), E_{out} is the total recoverable energy from the CDI cell (analogous to $E_{out,CDI}$ in Fig. 1A), and η is the recovery efficiency which represents the fraction of E_{out} recovered during discharge of the CDI cell.

The overall system efficiency $\eta_{sto+CDI}$ characterizes the energy recovered from $E_{in,CDI}$. However, the recovery efficiency η from Hawks et al. [52] should represent the energy recovered from $E_{out,CDI}$. Here, we propose a metric in agreement with the recovery efficiency η used to report the volumetric desalination energy of CDI. This metric is slightly different for storage and utilization of energy. For the case of energy storage, we refer to this metric as energy storage efficiency (or more briefly as storage efficiency). The storage efficiency is associated with the transfer of energy from the CDI cell into an energy storage device. We further define η_{sto} as the energy stored into the ES, $E_{ES,sto}$, divided by the maximum recoverable energy, $E_{out,CDI}$ (cf. Fig. 1B). Hence, the proposed energy storage efficiency enables the quantification of the recovered energy from the CDI operation.

The definition of storage efficiency η_{sto} and overall system efficiency $\eta_{sto+CDI}$ are also depicted in the schematic of Fig. 1C. This schematic presents a typical adsorption/desorption power curve in CDI, and the nearly linear power consumption profiles show a typical behavior for CDI at constant current operation. Our definition of the storage efficiency corresponds to the ratio of the energy delivered to the energy storage device $E_{ES,sto}$ (discharge area of power curve minus the energy losses, Fig. 1C main), over the recoverable energy from the discharge of the CDI cell $E_{out,CDI}$ (discharge area of power curve minus the energy losses, Fig. 1C inset). In contrast, the overall efficiency $\eta_{sto+CDI}$ is defined as $E_{ES,sto}$ over the total area during charge $E_{in,CDI}$ (Fig. 1C main).

2.2. Energy transfer for utilization (round-trip) in CDI

We here present an analysis of the storage and then reuse of the stored energy in a subsequent CDI adsorption cycle (Fig. 2). To complete the desalination cycle, we provide additional top-off energy, $E_\$$. This additional energy accounts for all the energy losses in the cycle and can be introduced directly to the CDI cell or into the energy storage device. Fig. 2A shows a schematic of the energy transfer for utilization from and to the CDI cell. The terms $E_{in,CDI}$, $E_{out,CDI}$, $E_{in,ES}$, and $E_{out,ES}$correspond to the total energy inputs or outputs to the components. Further, $E_{CDI,rec}$ and $E_{ES,sto}$ are the effective energy recovered into the CDI cell and the effective energy stored in the ES respectively. For instance, $E_{CDI,rec}$ is calculated as $E_{in,CDI}$ minus both the energy lost $E_{L,CDI,ch}$ during charge of the CDI cell and the top-off energy, $E_\$$.

Fig. 2B shows the comparison between utilization efficiency η_{util} and overall system efficiency $\eta_{util+CDI}$. The latter includes all the energy losses ($E_\$ = \sum_j E_{L,j}\ j = CDI, ES, DC-DC$) in the denominator, while the former includes only the losses due to both the DC-DC converter and the dissipation in the energy storage. Here we explicitly express utilization efficiency as

$$\eta_{util} = \frac{E_{CDI,rec}}{E_{out,CDI}} = \frac{E_{CDI,rec}}{E_{CDI,rec} + 2E_{L,DC-DC} + E_{L,ES,ch} + E_{L,ES,dis}}. \quad (1)$$

Note that in CDI studies, it is relevant to report volumetric

desalination efficiency, E_v. Therefore, the recovery efficiency metric, η, to report E_v should be η_{sto} or η_{util}, depending on the final use of the energy (storage or utilization).

3. Theory and simplified analytical approximation

Presented here are analytical and numerical tools to characterize the energy transfer process between a CDI cell and an SC (as the storage device) with a buck-boost converter (as the DC/DC converter). We neglect losses due to switching effects for three reasons. First, we assume moderate to low switching frequency, which is controlled by the inductance and current window. Second, the series resistance dominates energy losses over switching losses. Third, switching losses are approximately accounted by the model by using a resistor in series with the inductor. This resistance is assumed to account for all losses of the buck-boost converter.

3.1. Second order ODE model for energy transfer using a buck-boost converter

Fig. 3A shows a schematic of the circuit of a simplified buck-boost converter for energy transfer between a CDI cell (capacitance, C_{CDI}) and an SC (capacitance, C_{SC}). A set of two ODEs is used to predict the temporal evolution of charge in the left (CDI) and right (SC) circuit loop as follows

$$\begin{aligned} &L\ddot{q}_j + C_j\dot{q}_j + (R_j + R_L)q_j = 0, \\ &j = CDI, SC, \end{aligned} \tag{2}$$

where L is the inductance of the inductor that is located between the CDI and SC circuits. C_j and R_j are the capacitance and electrical series resistance of both the CDI cell (for $j = CDI$) and the supercapacitor (for $j = SC$). We implemented a MATLAB script to solve the two ODEs numerically. The overall structure of the code for the discharge of the CDI cell can be summarized as follows: first, the ODE for the CDI circuit is solved until the current in the circuit increases to I_1. At this point, the inductor is disconnected from the CDI circuit and connected to the SC circuit. Thereafter, the SC ODE equation is solved until the current decreases to I_2. The time spent during discharge at the CDI cell corresponds to the active discharge time step, $\Delta t_{on,dis}$, while the time spent during the charge of the SC is the inactive discharge time, $\Delta t_{off,dis}$. Since at each time step Δt a small amount of energy is transferred between circuits, the total number of switches to fully discharge the CDI cell varies with the magnitude L of the inductance and the current window $\Delta I = I_1 - I_2$. Fig. 3B shows a computed current profile as a function of time from the ODE model for typical CDI parameters. The overall structure described here is analogous for the charge of the CDI cell.

3.2. Analytical model for energy transfer using a buck-boost converter

Multiple approaches are available to derive analytical models for circuits. A common methodology to model buck-boost in CDI is a linearization of the potential at each Δt. With this simplification, one can iterate to find the final voltage in the SC to determine the total transfer time [39,40]. To derive an analytical model, we recognize that the magnitude of the inductance L has negligible effect on the total transfer time or final voltage in the SC (cf. Fig. S1 and associated discussion). This section presents a derivation of the analytical model for the discharge of the CDI cell, but the procedure is analogous for the charge of the cell. First, we approximate the total active and inactive time as

$$\begin{aligned} t_{on,dis} &= \sum_i \left(\Delta t_{on,dis}\right)_i = \frac{C_{CDI}\left(V_{CDI,i} - V_{CDI,f}\right)}{I_{mean}}, \\ t_{off,dis} &= \sum_i \left(\Delta t_{off,dis}\right)_i = \frac{C_{SC}\left(V_{SC,f} - V_{SC,i}\right)}{I_{mean}}, \\ t_{dis,total} &= t_{on,dis} + t_{off,dis}, \end{aligned} \tag{3}$$

where $V_{j,i}$ and $V_{j,f}$ ($j = SC, CDI$) are the initial and final voltage, respectively. The mean current, $I_{mean} = (I_1 + I_2)/2$ is an approximation of the actual value $I_{mean} = 1/\Delta t \int I(t)dt$, assuming approximately linear profiles for each phase. This assumption is not valid near energy depletion (~0 V) of the CDI cell. However, from an operational perspective of CDI (particularly without ion-selective membranes), the lower limit for voltage should be no less than ~0.2 V to ensure a high double layer efficiency [53].

We consider resistive energy losses of the form I^2Rt. Since current oscillates as a triangular wave (Fig. 3B), the triangular wave root mean square (RMS) current is an accurate representation for the energy losses as given by

$$I_{RMS} = \sqrt{I_{mean}^2 + \left(\frac{(I_1 - I_2)}{2\sqrt{3}}\right)^2}. \tag{4}$$

From energy conservation, the explicit expression for the available energy in the CDI cell transferred to the SC is then

$$\begin{aligned} \frac{1}{2}C_{SC}\left(V_{SC,f}^2 - V_{SC,i}^2\right) &= \frac{1}{2}C_{CDI}\left(V_{CDI,i}^2 - V_{CDI,f}^2\right) - I_{RMS}^2 R_{eq,CDI} t_{on,dis} - I_{RMS}^2 R_{eq,SC} t_{off,dis}, \\ &= E_{CDI,Avail} - I_{RMS}^2 R_{eq,SC} t_{off,dis}, \end{aligned} \tag{5}$$

where $R_{eq,j} = R_j + R_L$ ($j = CDI, SC$) is the equivalent series resistance. Combining equations (3)–(5), we obtain a second order algebraic equation with final voltage in the SC as the only unknown. Solving for $V_{SC,f}$ we derive a closed-form solution of the form

$$V_{SC,f} = \frac{\sqrt{C_{SC}^2\left(I_{RMS}^2 R_{eq,SC} + I_{mean}V_{SC,i}\right)^2 + 2E_{CDI,Avail}C_{SC}I_{mean}^2} - C_{SC}I_{RMS}^2 R_{eq,SC}}{C_{SC}I_{mean}}. \tag{6}$$

To determine the total energy transfer time, $t_{off,dis}$, we replace the final voltage in the SC (calculated from eq. (6)) in the discharge time equation (eq. (3)). Once we know the final voltage in the SC, the total energy loss E_{loss} is calculated as follows

$$E_{loss} = \left(\frac{1}{2}C_{CDI}\left(V_{CDI,i}^2 - V_{CDI,f}^2\right)\right) - \left(\frac{1}{2}C_{SC}\left(V_{SC,f}^2 - V_{SC,i}^2\right)\right). \tag{7}$$

Fig. 4A shows the final voltage in the supercapacitor computed with the analytical and ODE model as a function of the current window for different mean currents. The average relative difference between the models for the predicted final voltage in the SC is ~1%. This difference increases with ΔI and I_{mean} up to a maximum of ~5%. Fig. 4B shows the total transfer time computed with the models versus the current window for several I_{mean}. The total transfer time shows a good agreement between models, the average relative difference between the models for the predicted total transfer time is ~0.2%. Again, this difference increases with $\Delta I$and I_{mean} up to ~1%.

In section 1, we introduced the two possible scenarios for energy transfer, storage and utilization of energy. Here, we define storage η_{sto} and the overall system efficiency $\eta_{sto+CDI}$ in terms of the parameters from the analytical model as given by

$$\eta_{sto} = \frac{E_{in,ES}}{E_{in,ES} + E_{L,ES,ch}} = \frac{\left(\frac{1}{2}C_{SC}\left(V_{SC,f}^2 - V_{SC,i}^2\right)\right)}{\left(\frac{1}{2}C_{SC}\left(V_{SC,f}^2 - V_{SC,i}^2\right)\right) + \left(I_{RMS}^2 R_{eq,SC} t_{off,dis}\right)}, \tag{8}$$

and

$$\eta_{sto+CDI} = \frac{E_{in,ES}}{E_{in,ES} + E_{loss}} = \frac{\left(\frac{1}{2}C_{SC}\left(V_{SC,f}^2 - V_{SC,i}^2\right)\right)}{\left(\frac{1}{2}C_{SC}\left(V_{SC,f}^2 - V_{SC,i}^2\right)\right) + E_{loss}}. \tag{9}$$

Here, the generic subscript energy storage ES corresponds to the energy stored in the supercapacitor SC. Note that $R_{eq,SC}$ is used to calculate the energy losses due to the series resistance of the supercapacitor and resistance of the inductor. Finally, we calculate the utilization η_{util} and the overall system efficiency $\eta_{util+CDI}$ as

$$\eta_{util} = \frac{E_{CDI,rec}}{E_{CDI,rec} + E_{L,ES,ch} + E_{L,ES,dis}} = \frac{\left(\frac{1}{2}C_{SC}\left(V_{SC,f}^2 - V_{SC,i}^2\right)\right) - \left(I_{RMS}^2 R_{eq,CDI} t_{on,ch}\right) - \left(I_{RMS}^2 R_{eq,SC} t_{off,ch}\right)}{\left(\frac{1}{2}C_{SC}\left(V_{SC,f}^2 - V_{SC,i}^2\right)\right) - \left(I_{RMS}^2 R_{eq,CDI} t_{on,ch}\right) + \left(I_{RMS}^2 R_{eq,SC} t_{off,dis}\right)}, \tag{10}$$

and

$$\eta_{util+CDI} = \frac{E_{CDI,rec}}{E_{CDI,rec} + E_{loss}} = \frac{\left(\frac{1}{2}C_{SC}\left(V_{SC,f}^2 - V_{SC,i}^2\right)\right) - \left(I_{RMS}^2 R_{eq,CDI} t_{on,ch}\right) - \left(I_{RMS}^2 R_{eq,SC} t_{off,ch}\right)}{\left(\frac{1}{2}C_{SC}\left(V_{SC,f}^2 - V_{SC,i}^2\right)\right) - \left(I_{RMS}^2 R_{eq,CDI} t_{on,ch}\right) - \left(I_{RMS}^2 R_{eq,SC} t_{off,ch}\right) + E_{loss}}. \tag{11}$$

4. Energy recovery metrics for DC/DC buck-boost converter

Presented here are regimes in which a buck-boost converter will operate efficiently. The operational conditions required to discharge/charge a CDI cell at fixed productivity are first compared to a classic constant current operation. Then, the dynamics of the buck-boost converter operation are explored with respect to a constant current scheme. Also presented are a side-by-side comparison between the energy transfer efficiency for storage (one-way) and utilization (round-trip). Finally, engineering operational parameters are presented which help maximize the performance of the energy transfer process.

4.1. Charge or discharge conditions at fixed productivity

Productivity relates the treated water throughput to the projected area of the electrodes [52]. We here impose a condition of equal productivity for basis of comparison among charging and energy storage operations. To compare to typical research-type operation using a constant current source, we equate the constant current charging time to the total time used by the buck-boost circuit (i.e. the sum of the times the buck-boost converter is active and inactive). Note this basis of comparison penalizes the buck-boost circuit device for the time it spends delivering charge to the storage unit.

We first estimate the total charge transferred from the CDI to the SC as follows

$$q_{CDI} = C_{CDI}\left(V_{CDI,i} - V_{CDI,f}\right), \tag{12}$$

where q_{CDI} is the charge transferred from a cell of capacitance C_{CDI} with a voltage window from $V_{CDI,i}$ (CDI initial voltage) to $V_{CDI,f}$ (CDI final voltage). We set $V_{CDI,i}$ to 1 V to avoid Faradaic reactions at higher voltages, while $V_{CDI,f}$ is fixed to 0.4 V to avoid depletion of the electric double layers. The total time to transfer the energy from the CDI to the SC at constant current, I_{cc}, using a sourcemeter is given by

$$t_{cc,dis} = \frac{q_{CDI}}{I_{cc}}, \tag{13}$$

where $t_{cc,dis}$ corresponds to the total time to discharge the CDI cell at constant current with a sourcemeter. In contrast, when we incorporate a buck-boost converter to discharge (charge) the CDI cell, we introduce inactive time to the desalination cycle (Fig. 3B). The transfer time to deliver energy to the storage component then depends on the total charge stored into the SC. The charge stored in the SC is then as follows

$$q_{SC} = C_{SC}\left(V_{SC,f} - V_{SC,i}\right), \tag{14}$$

where the initial voltage $V_{SC,i}$ and capacitance C_{SC} are operational parameters. Note that the final voltage of the SC, $V_{SC,f}$ is calculated using eq. (6).

Next, the condition to maintain fixed productivity is derived by recognizing that the total time to discharge the CDI cell at constant current $t_{cc,dis}$ is equal to the total active and inactive time during discharge with a buck-boost converter, as given by

$$t_{cc,dis} = t_{on,dis} + t_{off,dis} = \frac{q_{CDI}}{I_{mean,P}} + \frac{q_{SC}}{I_{mean,P}}, \tag{15}$$

where $I_{mean,P}$ is the modified current for fixed productivity. Rearranging eq. (15) to find an explicit expression for $I_{mean,P}$ gives

$$I_{mean,P} = I_{cc}\left(\frac{q_{CDI} + q_{SC}}{q_{CDI}}\right) = I_{cc}\left(1 + \frac{q_{SC}}{q_{CDI}}\right). \tag{16}$$

We then rewrite the RMS current describing dissipative losses for the modified current at fixed productivity as in

$$I_{RMS,P} = \sqrt{I_{mean,P}^2 + \left(\frac{I_1 - I_2}{2\sqrt{3}}\right)^2}. \tag{17}$$

Solving the system of equations (6), (16) and (17), we can derive an expression that quantifies the proximity of the losses between source-meter and buck-boost converter discharge. This efficiency, which we term the constant current efficiency is given by

$$\eta_{cc}=\frac{I_{cc}^2(R_a+R_b+2R_c)(t_{cc,dis})}{I_{RMS,P}^2(R_a+R_b+2R_c)\left(t_{on,dis}+t_{off,dis}\right)}=\frac{I_{cc}^2}{\left(\left(I_{cc}\left(1+\frac{q_{SC}}{q_{CDI}}\right)\right)^2+\left(\frac{I_1-I_2}{2\sqrt{3}}\right)^2\right)}. \tag{18}$$

Note the latter analysis implies that the buck boost circuit operation is in a mid- to low-frequency region where specifically switching losses are negligible.

Fig. 5A main shows a plot of total transfer time during discharge (defined in eq. (7)) versus the initial voltage in the supercapacitor ranging from 0 to 5 V for 1, 2.5, 5, 10, 20, and 40 F values of capacitances. At constant mean current I_{mean}, the total time to discharge the CDI cell increases at low initial voltages and high capacitances in the SC. This effect is primarily due to a rise in the total charge accumulated in the SC (eq. (14)). This is attributed to a higher C_{SC} and to an increment of the difference between $V_{SC,f}$ (eq. (6)) and $V_{SC,i}$ for decreasing values of $V_{SC,i}$. Fig. 5A inset shows the total dissipative losses (eq. (7)) for $V_{SC,i}$ from 0 to 5 V for SC capacitances of 1, 2.5, 5, 10, 20, and 40 F. Similar to the total transfer time, the increase in the total transfer time at low values of $V_{SC,i}$ leads to higher energy loss E_{loss} in the energy transfer process.

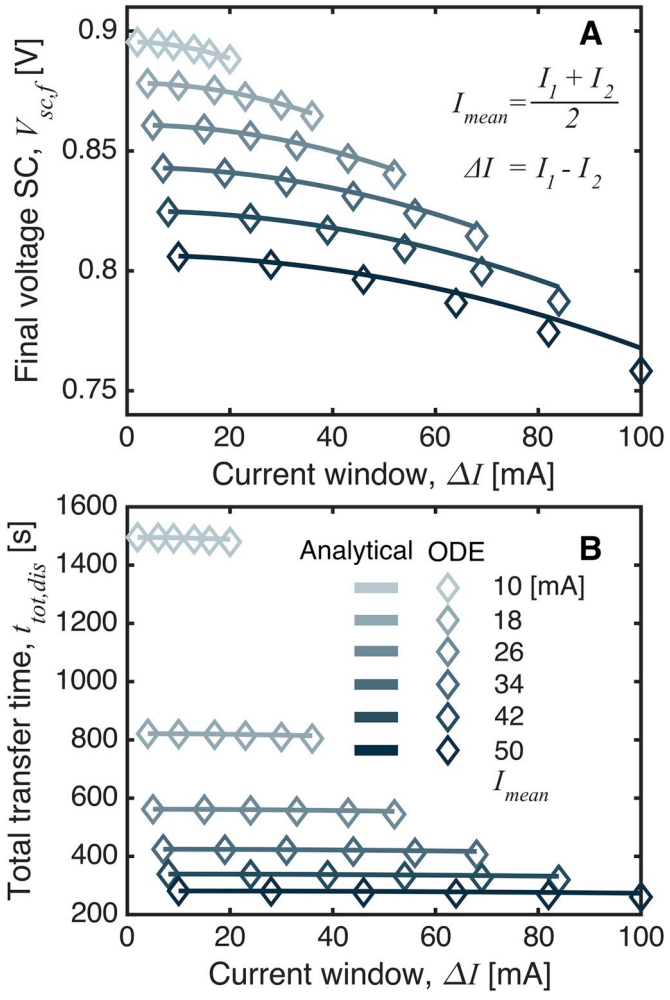

Fig. 4. Comparison of the final voltage in the SC (**A**) and the total transfer time (**B**) between the second order ODE model (symbols) and the analytical model approximation (solid lines) as a function of the current window $I_1 - I_2$ (ΔI) and for various mean current values, I_{mean}. Both simulations use the same input parameters: $C_{CDI} = C_{SC} = 10$ F, $V_{CDI,i} = 1$ V, $V_{CDI,f} = 0.4$ V, $V_{SC,i} = 0$ V, $R_{CDI} = 3\,\Omega$, $R_{SC} = 0.1\,\Omega$, and $R_L = 0.01\,\Omega$. An inductance of $L = 100$ mH was used in the second order ODE simulation.

Fig. 5B main shows the modified mean current at fixed productivity versus the initial voltage in the supercapacitor ranging from 0 to 5 V for SC capacitances values of 1, 2.5, 5, 10, 20, and 40 F compared to a constant current discharge at $I_{cc} = 30\ mA$. The modified current $I_{mean,P}$ increases for low initial voltages and high capacitances in the SC. This increase is attributable to the one-to-one correlation with the transfer time. That is, the higher the transfer time, the higher the modified current for fixed productivity and vice versa. Fig. 5B inset shows the final voltage in the SC versus the initial voltage in the supercapacitor for different capacitances. The value of $V_{SC,f}$ gets closer to $V_{SC,i}$ for high values of both $V_{SC,i}$ and C_{SC}. Also, storing charge at higher voltages implies less current to transfer the same energy, therefore less energy loss.

The main plot of Fig. 5C shows the total transfer time as a function of the initial voltage in the supercapacitor (ranging from 0 to 5 V) for 1, 2.5, 5, 10, 20, and 40 F values of capacitance, when the modified current $I_{mean,P}$ (for fixed productivity) is used instead of the constant mean current $I_{mean} = 30$ mA (as in Fig. 5A). Since productivity is kept constant, the transfer times collapse to 200 s as this is the time to transfer q_{CDI} from the CDI cell at I_{cc}. The latter collapse holds for all initial voltages and capacitances of the SC. Moreover, this collapse is a result of the restriction for transfer time imposed in equation (15). The inset of Fig. 5C shows energy lost versus $V_{SC,i}$ and C_{SC}. The energy loss trends are similar to the energy losses from Fig. 1C; but the magnitudes are higher due to the increase in the modified mean current associated with the assumption of fixed productivity.

Fig. 5D shows the constant current efficiency (defined in eq. (18)) for a fixed current window ΔI versus the initial voltage in the supercapacitor ranging from 0 to 5 V for 1, 2.5, 5, 10, 20, and 40 F values of capacitance. η_{cc} quickly decreases for low initial voltages in the SC. This decrease is attributable to the increase of the modified current at fixed productivity for lower values of $V_{SC,i}$.

Fig. 6A shows the energy losses (eq. (7)) as a function of the mean current at constant current and voltage window. The energy loss for a given I_{cc} increases with the current windows ΔI. However, the extra dissipative loss due to a higher current window is at most ~25% more than the energy loss at $\Delta I = 0$. Fig. 6B shows the inactive time (the time spent in the SC during discharge/charge of the CDI cell) versus the current I_{cc} and current window ΔI. Inactive time decreases with either high I_{cc} or ΔI, as expected. High current translates into more energy loss and, hence, less available energy to transfer from the CDI cell to the SC and an associated reduction in the inactive time. Finally, Fig. 6C shows the constant current efficiency versus the current I_{cc} and current window ΔI. For a fixed I_{cc}, a high current window shows a decrease in the η_{cc}. At first glance, eq. (18) might suggest that the buck-boost converter should be operated with the smallest possible current window. However, smaller current windows increase the number of switches required to transfer the same amount of energy. Therefore, a limiting factor in choosing ΔI is the potential increase in switching losses (which are neglected here).

4.2. Storage (one-way) versus utilization (round-trip) energy transfer efficiency

Discussed here are the comparison and contrast of the energy transfer efficiencies for storage (one-way) and utilization (round-trip). Considered are conservative yet realistic values for the series resistances of 10 Ω and 1 Ω for the CDI and SC, respectively.

The main plot of Fig. 7A shows the storage efficiency (eq. (8)) versus the initial voltage in the supercapacitor (ranging from 0 to 5 V) for 1, 2.5, 5, 10, 20, and 40 F values of capacitance. Storage efficiency

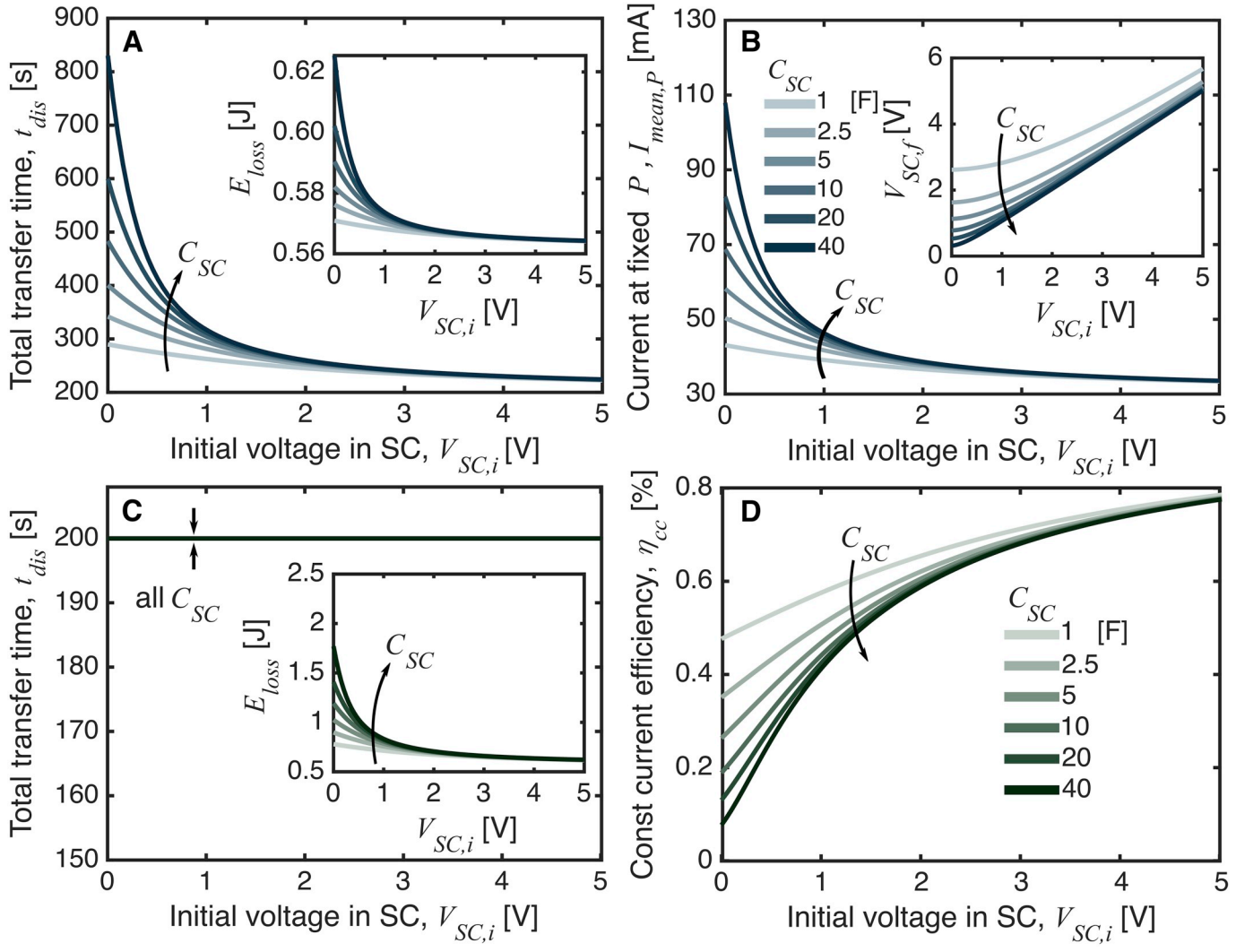

Fig. 5. (**A**) (main) Total time to transfer energy from a CDI cell to an SC using a buck-boost converter as a function of the initial voltage in the SC for several SC capacitances, C_{SC}. Transfer time approaches 200 s, which is the time to discharge the CDI cell at $I_{mean} = 30$ mA. (inset) Energy losses versus the initial voltage in the SC at $I_{mean} = 30$ mA. (**B**) (main) Modified current to discharge the CDI into an SC at a productivity equivalent to a constant current discharge at 30 mA. (inset) The final voltage of the SC versus the initial voltage in the SC for the modified current. (**C**) (main) Total transfer time versus initial voltage in the SC using the modified current for fixed productivity. (inset) Energy losses versus the initial voltage in the SC with the modified current. (**D**) The efficiency η_{cc} for the proximity between constant current discharge and buck-bust converter discharge as a function of the initial voltage in the SC and several C_{SC}. Fixed parameters used in this figure: $C_{CDI} = 10$ F, $V_{CDI,i} = 1$ V, $V_{CDI,f} = 0.4$ V, $\Delta I = 20$ mA, $R_{CDI} = 3\ \Omega$, $R_{SC} = 0.1\ \Omega$, and $R_L = 0.01\ \Omega$.

decreases for decreasing values of $V_{SC,i}$ and high C_{SC}. η_{sto} shows the highest numerical values among all of the considered efficiency metrics. This is expected as the energy lost during the charge of the SC is the only loss adversely affecting η_{sto}. The inset of Fig. 7A shows the overall system efficiency $\eta_{sto+CDI}$ (eq. (9)) versus $V_{SC,i}$ for 1, 2.5, 5, 10, 20, and 40 F values of C_{SC}. The trend of $\eta_{sto+CDI}$ as a function of the initial voltage and capacitance of the SC shows a similar behavior than the trend for η_{sto}. However, the magnitude of $\eta_{sto+CDI}$ is significantly lower than η_{sto} as the former also considered desalination losses. In fact, the system efficiency $\eta_{sto+CDI}$ (sometimes imprecisely called energy recovery efficiency [38–41,43,45,46]) is about half of the magnitude of storage efficiency η_{sto} for the chosen realistic parameters.

The main plot of Fig. 7B shows the utilization (round-trip) efficiency (as per eq. (10)) as a function of the initial voltage in the SC and SC capacitances of 1, 2.5, 5, 10, 20, and 40 F. Utilization efficiency decreases at high values of C_{SC} and low values of the $V_{SC,i}$. η_{util} shows lower values of efficiency than η_{sto}, as utilization efficiency takes into account the charge and discharge losses associated with the SC. However, for a $V_{SC,i}$ of 1 V or higher, η_{util} shows efficiency magnitudes of ~90% for all the capacitances ranging from 1 to 40 F. The inset of Fig. 7B shows the overall system efficiency $\eta_{util+CDI}$ (eq. (11)) versus $V_{SC,i}$ for C_{SC} of 1, 2.5, 5, 10, 20, and 40 F. The system efficiency $\eta_{util+CDI}$, again similar to η_{util}, decreases with low initial voltages or high capacitances in the SC. However, the overall system efficiency $\eta_{util+CDI}$ includes all the terms for energy losses in the system and therefore represents the overall system efficiency when a buck-boost converter is used to recover energy. As expected, the system efficiency $\eta_{util+CDI}$ also shows the lowest efficiency magnitude among the four energy transfer efficiency metrics (eqs. (8)–(11)). Lastly, the energy losses associated with the CDI series resistance (included in $\eta_{util+CDI}$ and $\eta_{sto+CDI}$) penalizes only the available energy to recover, and not the efficiency of the recovery process with a buck-boost converter.

In summary, high recovery efficiencies (for both storage and utilization) from (and to) a CDI cell with a buck-boost converter can be achieved, even taking into account dissipative losses in the cell. For instance, at $V_{SC,i}$ of 1 V and C_{SC} from 1 to 40 F, the storage η_{sto} and utilization efficiencies η_{util} are ~95% and ~90%, respectively.

4.3. Engineering estimates for energy transfer efficiency in CDI

Presented here is a discussion of the effect of the mean current magnitude and SC series resistance on the storage and utilization efficiencies. The initial voltage of SC is assumed to be $V_{SC,i} = 0$ V. Note that higher values of $V_{SC,i}$ result in higher efficiencies (Fig. S2).

Fig. 8A shows the storage efficiency versus the mean current I_{mean} values ranging from 1 to 50 mA for SC capacitances of 1, 2.5, 5, 10, 20, and 40 F. Storage efficiency η_{sto} increases for lower values of capacitance. Each curve of η_{sto} as a function of I_{mean} at a fixed C_{SC} exhibits a local maximum (efficiency peak) at I_{mean} near ~7 mA. The efficiency peak is a consequence of a decrease in the energy lost near I_{mean} of ~7 mA; therefore, the peak in efficiency is attributable to the behavior of energy lost as a function of I_{mean}. Two parameters regulate the losses, namely, the total transfer time and the magnitude of the mean current. For fixed series resistances the model predicts an increase in the energy lost as I_{mean} approaches zero. This increase in the dissipative losses is sublinear with respect to total transfer time at lower mean currents, hence the efficiency η_{sto} diminishes at low I_{mean}. On the other hand, the energy lost scales with I^2; and so, higher mean current results in a rise in the energy dissipated. Simultaneously, the total transfer time reaches a plateau as mean current increases. As a consequence, there are higher energy losses at either high I_{mean} values or as I_{mean} approaches zero (with a local maximum at moderate mean currents ~7 mA). Fig. 8C shows the utilization efficiency η_{util} versus the mean current for C_{SC} of 1, 2.5, 5, 10, 20, and 40 F. Utilization efficiency η_{util} (similar to η_{sto}) increases for lower C_{SC} and exhibits an efficiency peak. The reasons for the local maximum in η_{util} are analogous to that of η_{sto}. However, utilization efficiency η_{util} does show a more rapid decay of efficiency than storage efficiency η_{sto} for decreasing the initial voltage in the SC.

Fig. 8B shows storage efficiency as a function of the series resistance in the SC and C_{SC} of 1, 2.5, 5, 10, 20, and 40 F. As expected, η_{sto} shows a monotonic decrease for increasing SC resistances. Moreover, the reduction in efficiency is strongly affected by the capacitance of the supercapacitor with higher capacitance causing lower efficiency. This effect of C_{SC} on η_{sto} is explained with the increase in the total energy lost (eq. (7)) for higher values of C_{SC} (Fig. 5A inset). Fig. 8D shows utilization efficiency versus R_{SC} for SC capacitances of 1, 2.5, 5, 10, 20, and 40 F.

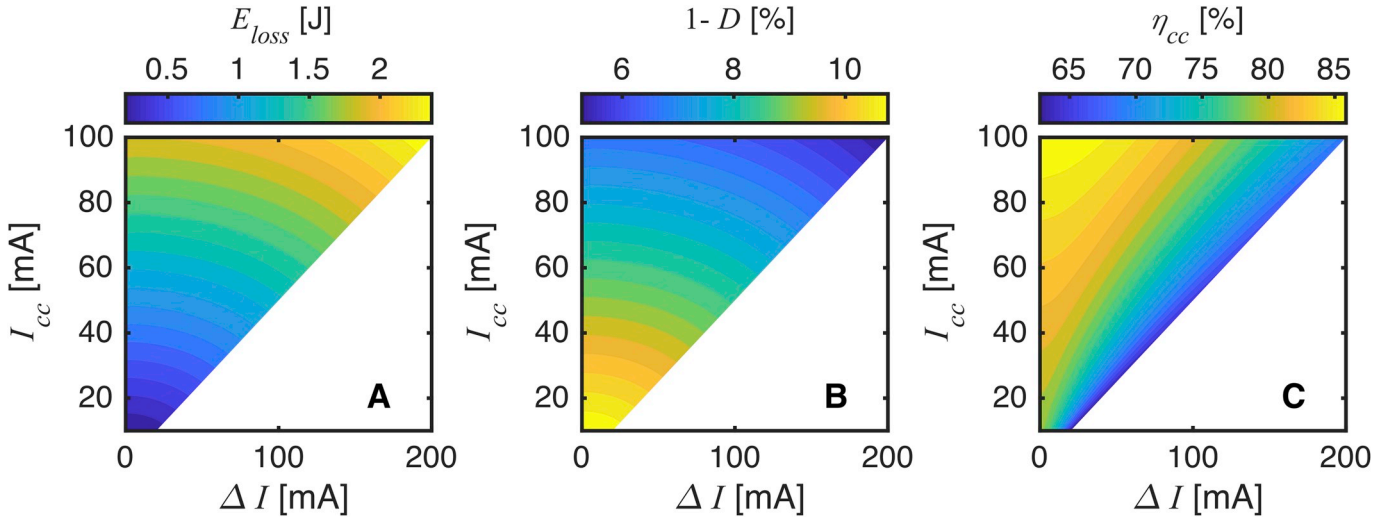

Fig. 6. (**A**) Contour plot of energy losses (defined in eq. (7)) for several I_{cc} and ΔI values. (**B**) Contour plot of the inactive duty cycle for different values of I_{cc} and ΔI. (**C**) Contour plot of efficiency of the proximity between constant current discharge with buck-boost converter discharge, η_{cc}, for different values of I_{cc} and ΔI. Fixed parameters used in this figure: $C_{CDI} = 10$ F, $V_{CDI,i} = 1$ V, $V_{CDI,f} = 0.4$ V, $C_{SC} = 1$ F, $V_{SC,i} = 5$ V, $R_{CDI} = 3\ \Omega$, $R_{SC} = 0.1\ \Omega$, and $R_L = 0.01\ \Omega$.

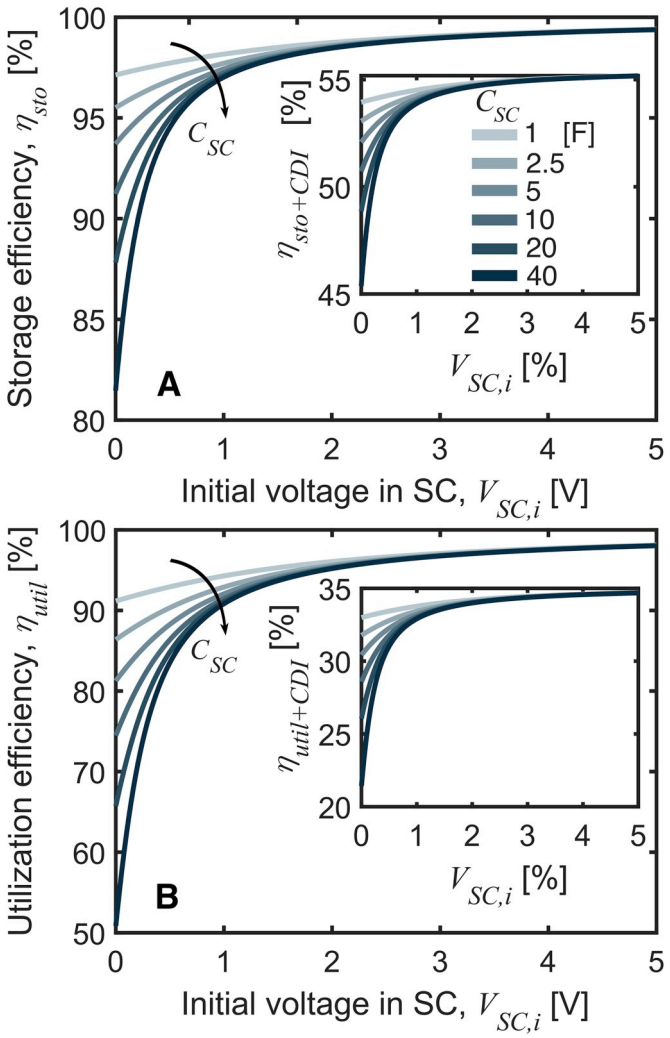

Fig. 7. (**A**) (main) Storage (one-way) efficiency (eq. (8)) as a function of initial voltage in SC. (inset) The system efficiency for desalination and storage $\eta_{sto+CDI}$ (eq. (9)) as a function of $V_{SC,i}$. (**B**) (main) Utilization (round-trip) efficiency (eq. (10)) as a function of initial voltage in SC. (inset) The system efficiency for desalination and utilization $\eta_{util+CDI}$ (eq. (11)) as function $V_{SC,i}$. Fixed parameters used in this figure: $C_{CDI} = 10$ F, $V_{CDI,i} = 1$ V, $V_{CDI,f} = 0.4$ V, $I_{mean} = 30$ mA, $\Delta I = 20$ mA $R_{CDI} = 10\ \Omega$, $R_{SC} = 1\ \Omega$, and $R_L = 0.01\ \Omega$.

Like η_{sto}, utilization efficiency η_{util} monotonically decreases at higher R_{SC}. Lastly, utilization efficiency compared to storage efficiency shows overall a lower magnitude for all the capacitances and resistances of the SC.

4.4. Desalination performance with buck-boost

We coupled the current model to a model for the dynamics of a CDI [54] in order to evaluate desalination performance metrics for a CDI cell/storage system. The buck-boost converter output is taken as the forcing function of the cell desalination model. The converter output considered here is approximately a constant current operation but also contains some high-frequency elements associated buck-boost operation. Section 3 of the SI summarizes the results of these simulations. Also presented is a comparison of the classic constant current operation with CDI/storage system. Importantly, this comparison is performed assuming equal salt concentration reduction and equal productivity. To take into account the "down time" associated with power transfer, equal productivity is achieved by increasing the instantaneous currents (and hence instantaneous power dissipation) supplied to the CDI cell in the CDI/storage system. Despite the non-ideal components of the forcing function, energy recovery with a buck-boost converter shows significantly improved energy performance for the overall system. For fixed productivity and a series resistance of 5 Ω, the simulation suggests a 1.4x decrease in system volumetric energy consumption relative to standard CDI cell operation without energy transfer. For a CDI cell with only 1 Ω series resistance, the system volumetric energy consumption is decreased by a factor of 4.7. See Section 3 of the SI for further details including CDI parameters and model assumptions.

5. Conclusions

We defined and compared efficiency metrics that account for energy storage (one-way) and energy utilization (round-trip) in CDI. These efficiency metrics account for the energy transfer between a CDI cell and a generic energy storage device using a DC/DC converter. We compared the recovery efficiency metrics (η_{sto} and η_{util}) to metrics accounting for overall system efficiency ($\eta_{sto+CDI}$ and $\eta_{util+CDI}$). For the quantification of the various efficiencies, we derived an analytical model with closed-form expressions for the energy transfer between a CDI cell to an SC (as the energy storage device) using a buck-boost converter. We benchmarked this analytical model with a numerical model leveraging a direct and accurate prediction of the energy transfer with the buck-boost converter. We also proposed a methodology in which the CDI cell is operated with the aid of a buck-boost converter at constant productivity compared to the constant current operation. To this end, we defined a metric called constant current efficiency η_{cc} to quantify the comparison between the constant current energy losses (best-case scenario) and the energy losses due to buck-boost operation (which requires higher mean currents to decrease the total transfer time to match productivity).

The analytical model showed good agreement with the numerical model for several current windows and mean currents. The relative difference between models was ~0.2% for the total transfer time and ~1% for the final voltage in the SC. Using the analytical model, we found that the total transfer time increases at low initial voltages and high capacitances in the SC. This increase in transfer time was attributed to an increment in the total charge accumulated in the SC for low $V_{SC,i}$ and high C_{SC}. To decrease the transfer time (for fixed productivity), we found that a higher modified mean current is needed for longer periods of total transfer time (and vice versa). Using $I_{mean,P}$, the constant current efficiency η_{cc} was ~80% for an initial voltage of ~5 V in the SC.

As expected, the overall system efficiencies ($\eta_{sto+CDI}$ and $\eta_{util+CDI}$) were significantly lower than the storage and utilization efficiencies (η_{sto} and η_{util}) for a CDI cell series resistance of 10 Ω. Even at high CDI series resistances, the model predicted storage η_{sto} and utilization efficiencies η_{util} of ~95% and ~90%, respectively (for an initial voltage in the SC of 1 V and SC capacitances from 1 to 40 F). For the same operational parameters, the efficiencies $\eta_{sto+CDI}$ and $\eta_{util+CDI}$ were ~54% and ~34%, respectively. The energy lost in the overall desalination system due to the CDI series resistance penalizes only the available energy to recover and does add additional penalty (over a standard CDI) to the recovery process. Therefore, we recommend employing either storage η_{sto} or utilization η_{util} efficiency as the recovery efficiency [52] to calculate the recovered energy from CDI when reporting volumetric desalination E_v energy.

Declaration of competing interest

The authors declare that they have no known competing financial interests or personal relationships that could have appeared to influence the work reported in this paper.

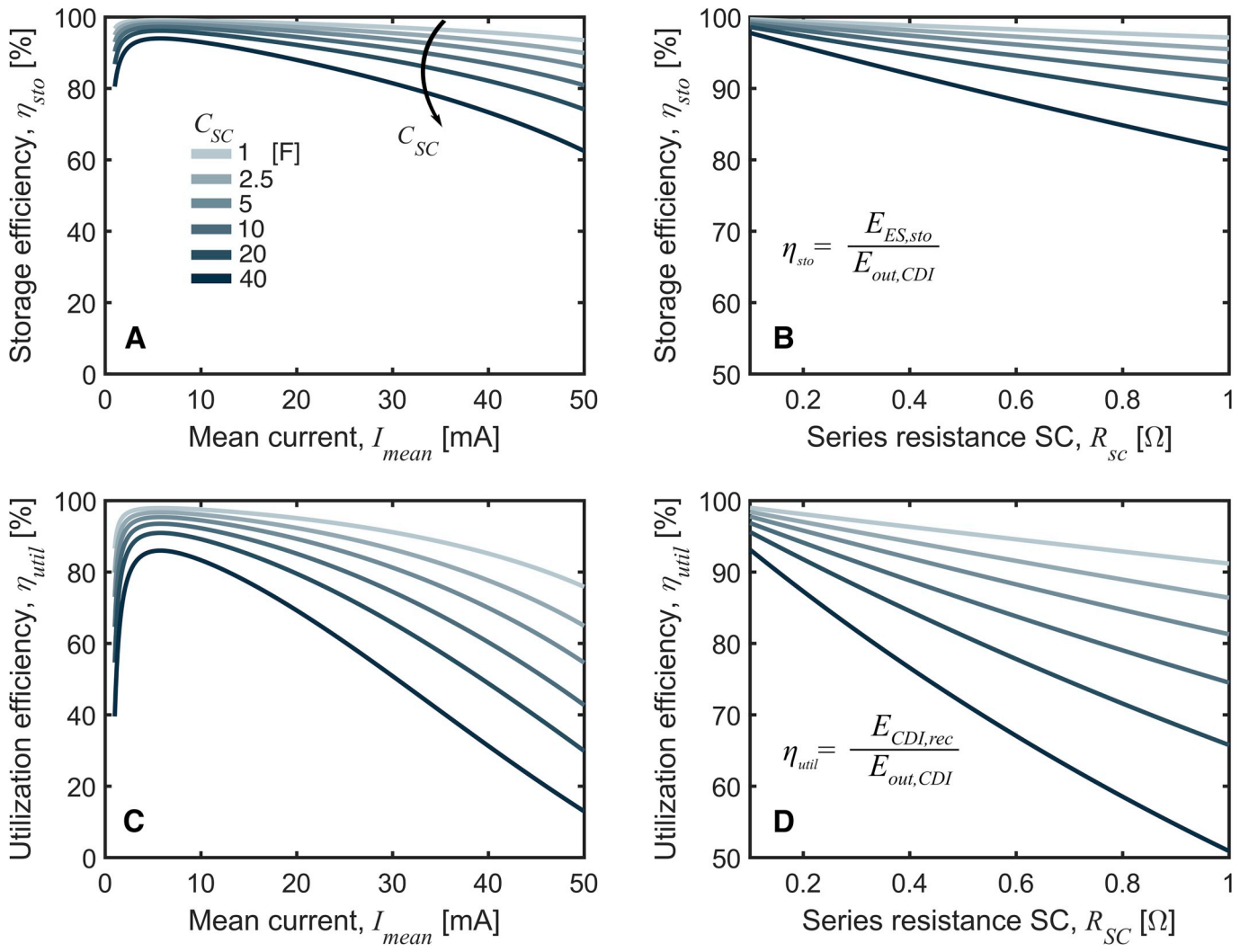

Fig. 8. (**A**) Storage efficiency (from eq. (8)) as a function of mean current at $R_{SC} = 1\ \Omega$. (**B**) Storage efficiency as a function of series resistance in the SC at $I_{mean} = 30$ mA. (**C**) Utilization efficiency (from eq. (10)) as a function of mean current at $R_{SC} = 1\ \Omega$. (**D**) Storage efficiency as a function of series resistance in the SC at $I_{mean} = 30$ mA. Fixed parameters used in this figure are as follows: $C_{CDI} = 10$ F, $V_{CDI,i} = 1$ V, $V_{CDI,f} = 0.4$ V, $V_{SC,i} = 0$ V, $\Delta I = 20$ mA $R_{CDI} = 10\ \Omega$, and $R_L = 0.01\ \Omega$.

Acknowledgments

D.I.O would like to thank the support of CONICYT - Becas Chile/72160536. Work at LLNL was performed under the auspices of the US DOE by LLNL under Contract DE-AC52-07NA27344, LDRD by LLNL under Contract 18-ERD-024, and CEC under Contract ECP16-014.

Appendix A. Supplementary data

Supplementary data to this article can be found online at https://doi.org/10.1016/j.jpowsour.2019.227409.

References

[1] M.M. Mekonnen, A.Y. Hoekstra, Four billion people facing severe water scarcity, Sci. Adv. 2 (2) (2016), e1500323, https://doi.org/10.1126/sciadv.1500323.
[2] M. Hightower, S.A. Pierce, The energy challenge, Nature 452 (7185) (2008) 285–286, https://doi.org/10.1038/452285a.
[3] M.S. Mohsen, O.R. Al-Jayyousi, Brackish water desalination: an alternative for water supply enhancement in Jordan, Desalination 124 (1–3) (1999) 163–174, https://doi.org/10.1016/S0011-9164(99)00101-0.
[4] K. Walha, R Ben Amar, L. Firdaous, F. Quéméneur, P. Jaouen, Brackish groundwater treatment by nanofiltration, reverse osmosis and electrodialysis in Tunisia: performance and cost comparison, Desalination 207 (1–3) (2007) 95–106, https://doi.org/10.1016/j.desal.2006.03.583.
[5] A. Subramani, J.G. Jacangelo, Emerging desalination technologies for water treatment: a critical review, Water Res. 75 (2015) 164–187, https://doi.org/10.1016/j.watres.2015.02.032.
[6] S. Manju, N. Sagar, Renewable energy integrated desalination: a sustainable solution to overcome future fresh-water scarcity in India, Renew. Sustain. Energy Rev. 73 (January 2016) (2017) 594–609, https://doi.org/10.1016/j.rser.2017.01.164.
[7] A. Ramachandran, D.I. Oyarzun, S.A. Hawks, P.G. Campbell, M. Stadermann, J. G. Santiago, Comments on "Comparison of energy consumption in desalination by capacitive deionization and reverse osmosis.", Desalination 461 (March) (2019) 30–36, https://doi.org/10.1016/j.desal.2019.03.010.
[8] A. Hemmatifar, A. Ramachandran, K. Liu, D.I. Oyarzun, M.Z. Bazant, J.G. Santiago, Thermodynamics of ion separation by electrosorption, Environ. Sci. Technol. 52 (2018) 10196–10204, https://doi.org/10.1021/acs.est.8b02959.
[9] A. Ramachandran, D.I. Oyarzun, S.A. Hawks, M. Stadermann, J.G. Santiago, High water recovery and improved thermodynamic efficiency for capacitive deionization using variable flowrate operation, Water Res. 155 (2019) 76–85, https://doi.org/10.1016/j.watres.2019.02.007.
[10] Y. Oren, Capacitive deionization (CDI) for desalination and water treatment — past, present and future (a review), Desalination 228 (1–3) (2008) 10–29, https://doi.org/10.1016/j.desal.2007.08.005.
[11] M.a. Anderson, A.L. Cudero, J. Palma, Capacitive deionization as an electrochemical means of saving energy and delivering clean water. Comparison to present desalination practices: will it compete? Electrochim. Acta 55 (12) (2010) 3845–3856, https://doi.org/10.1016/j.electacta.2010.02.012.

[12] P. Xu, J.E. Drewes, D. Heil, G. Wang, Treatment of brackish produced water using carbon aerogel-based capacitive deionization technology, Water Res. 42 (10–11) (2008) 2605–2617, https://doi.org/10.1016/j.watres.2008.01.011.
[13] R.T. Mayes, C. Tsouris, J.O. Kiggans, S.M. Mahurin, D.W. Depaoli, S. Dai, Hierarchical ordered mesoporous carbon from phloroglucinol-glyoxal and its application in capacitive deionization of brackish water, J. Mater. Chem. 20 (39) (2010) 8674–8678, https://doi.org/10.1039/c0jm01911a.
[14] Y.-J. Kim, J.-H. Choi, Selective removal of nitrate ion using a novel composite carbon electrode in capacitive deionization, Water Res. 46 (18) (2012) 6033–6039, https://doi.org/10.1016/j.watres.2012.08.031.
[15] C.-H. Hou, C.-Y. Huang, A comparative study of electrosorption selectivity of ions by activated carbon electrodes in capacitive deionization, Desalination 314 (2013) 124–129, https://doi.org/10.1016/j.desal.2012.12.029.
[16] Y.J. Kim, J.H. Kim, J.H. Choi, Selective removal of nitrate ions by controlling the applied current in membrane capacitive deionization (MCDI), J. Membr. Sci. 429 (2013) 52–57.
[17] J. Yang, L. Zou, N.R. Choudhury, Ion-selective carbon nanotube electrodes in capacitive deionisation, Electrochim. Acta 91 (2013) 11–19, https://doi.org/10.1016/j.electacta.2012.12.089.
[18] D.I. Oyarzun, A. Hemmatifar, J.W. Palko, M. Stadermann, J.G. Santiago, Ion selectivity in capacitive deionization with functionalized electrode: theory and experimental validation, Water Res. X 1 (2018) 100008, https://doi.org/10.1016/j.wroa.2018.100008.
[19] J.W. Palko, D.I. Oyarzun, B. Ha, M. Stadermann, J.G. Santiago, Nitrate removal from water using electrostatic regeneration of functionalized adsorbent, Chem. Eng. J. 334 (2018) 1289–1296, https://doi.org/10.1016/j.cej.2017.10.161.
[20] D.I. Oyarzun, A. Hemmatifar, J.W. Palko, M. Stadermann, J.G. Santiago, Adsorption and capacitive regeneration of nitrate using inverted capacitive deionization with surfactant functionalized carbon electrodes, Separ. Purif. Technol. 194 (June 2017) (2018) 410–415, https://doi.org/10.1016/j.seppur.2017.11.027.
[21] S.A. Hawks, M.R. Cerón, D.I. Oyarzun, et al., Using ultramicroporous carbon for the selective removal of nitrate with capacitive deionization, Environ. Sci. Technol. (June 2019), https://doi.org/10.1021/acs.est.9b01374 acs.est.9b01374.
[22] F.A. AlMarzooqi, A.A. Al Ghaferi, I. Saadat, N. Hilal, Application of Capacitive Deionisation in water desalination: a review, Desalination 342 (2014) 3–15, https://doi.org/10.1016/j.desal.2014.02.031.
[23] S. Porada, R. Zhao, A. Van Der Wal, V. Presser, P.M. Biesheuvel, Review on the science and technology of water desalination by capacitive deionization, Prog. Mater. Sci. 58 (8) (2013) 1388–1442, https://doi.org/10.1016/j.pmatsci.2013.03.005.
[24] J.E. Dykstra, S. Porada, A. van der Wal, P.M. Biesheuvel, Energy consumption in capacitive deionization – constant current versus constant voltage operation, Water Res. 143 (2018) 367–375, https://doi.org/10.1016/j.watres.2018.06.034.
[25] J. Kang, T. Kim, K. Jo, J. Yoon, Comparison of salt adsorption capacity and energy consumption between constant current and constant voltage operation in capacitive deionization, Desalination 352 (2014) 52–57, https://doi.org/10.1016/j.desal.2014.08.009.
[26] Y. Qu, P.G. Campbell, L. Gu, et al., Energy consumption analysis of constant voltage and constant current operations in capacitive deionization, Desalination 400 (2016) 18–24, https://doi.org/10.1016/j.desal.2016.09.014.
[27] A. Ramachandran, S.A. Hawks, M. Stadermann, J.G. Santiago, Frequency analysis and resonant operation for efficient capacitive deionization, Water Res. 144 (9) (2018) 581–591, https://doi.org/10.1016/j.watres.2018.07.066.
[28] R. Zhao, O. Satpradit, H.H.M. Rijnaarts, P.M. Biesheuvel, A. van der Wal, Optimization of salt adsorption rate in membrane capacitive deionization, Water Res. (2013), https://doi.org/10.1016/j.watres.2013.01.025.
[29] S.J. Seo, H. Jeon, J.K. Lee, et al., Investigation on removal of hardness ions by capacitive deionization (CDI) for water softening applications, Water Res. 44 (7) (2010) 2267–2275, https://doi.org/10.1016/j.watres.2009.10.020.
[30] Y.A.C. Jande, W.S. Kim, Desalination using capacitive deionization at constant current, Desalination 329 (2013) 29–34, https://doi.org/10.1016/j.desal.2013.08.023.
[31] P.M. Biesheuvel, A. van der Wal, Membrane capacitive deionization, J. Membr. Sci. 346 (2) (2010) 256–262, https://doi.org/10.1016/j.memsci.2009.09.043.
[32] H. Li, L. Zou, Ion-exchange membrane capacitive deionization: a new strategy for brackish water desalination, Desalination 275 (1–3) (2011) 62–66, https://doi.org/10.1016/j.desal.2011.02.027.
[33] D. Dondi, A. Bertacchini, D. Brunelli, L. Larcher, L. Benini, Modeling and optimization of a solar energy harvester system for self-powered wireless sensor networks, IEEE Trans. Ind. Electron. 55 (7) (2008) 2759–2766, https://doi.org/10.1109/TIE.2008.924449.
[34] K. Kobayashi, H. Matsuo, Y. Sekine, Novel solar-cell power supply system using a multiple-input DC–DC converter, IEEE Trans. Ind. Electron. 53 (1) (2006) 281–286, https://doi.org/10.1109/TIE.2005.862250.
[35] K.K. Win, S. Dasgupta, S.K. Panda, An optimized MPPT circuit for thermoelectric energy harvester for low power applications, in: 8th Int Conf Power Electron - ECCE Asia "Green World with Power Electron ICPE 2011-ECCE Asia, 2011, pp. 1579–1584, https://doi.org/10.1109/ICPE.2011.5944535.
[36] S.K. Changchien, T.J. Liang, J.F. Chen, L.S. Yang, Novel high step-up DCDC converter for fuel cell energy conversion system, IEEE Trans. Ind. Electron. 57 (6) (2010) 2007–2017, https://doi.org/10.1109/TIE.2009.2026364.
[37] M. Nymand, M.A.E. Andersen, High-efficiency isolated boost DCDC converter for high-power low-voltage fuel-cell applications, IEEE Trans. Ind. Electron. 57 (2) (2010) 505–514, https://doi.org/10.1109/TIE.2009.2036024.
[38] J. Kang, T. Kim, H. Shin, J. Lee, J.-I. Ha, J. Yoon, Direct energy recovery system for membrane capacitive deionization, Desalination 398 (2016) 144–150, https://doi.org/10.1016/j.desal.2016.07.025.
[39] A.M. Pernía, J.G. Norniella, J.A. Martín-Ramos, J. Díaz, J.A. Martínez, Up-down converter for energy recovery in a CDI desalination system, IEEE Trans. Power Electron. 27 (7) (2012) 3257–3265, https://doi.org/10.1109/TPEL.2011.2180926.
[40] A.M. Pernia, F.J. Alvarez-Gonzalez, M.A.J. Prieto, P.J. Villegas, F. Nuno, New control strategy of an up-down converter for energy recovery in a CDI desalination system, IEEE Trans. Power Electron. 29 (7) (2014) 3573–3581, https://doi.org/10.1109/TPEL.2013.2280814.
[41] M. Alkuran, M. Orabi, N. Scheinberg, Highly efficient Capacitive De-Ionization (CDI) water purification system using a buck-boost converter, in: 2008 Twenty-Third Annual IEEE Applied Power Electronics Conference and Exposition, vol. 1, IEEE, 2008, pp. 1926–1930, https://doi.org/10.1109/APEC.2008.4522991.
[42] J. Landon, X. Gao, J.K. Neathery, K. Liu, Energy recovery in parallel capacitive deionization operations, ECS Trans. 53 (30) (2013) 235–243, https://doi.org/10.1149/05330.0235ecst.
[43] L. Chen, X. Yin, L. Zhu, Y. Qiu, Energy recovery and electrode regeneration under different charge/discharge conditions in membrane capacitive deionization, Desalination 439 (April) (2018) 93–101, https://doi.org/10.1016/j.desal.2018.04.012.
[44] C. Tan, C. He, W. Tang, P. Kovalsky, J. Fletcher, T.D. Waite, Integration of photovoltaic energy supply with membrane capacitive deionization (MCDI) for salt removal from brackish waters, Water Res. 147 (2018) 276–286, https://doi.org/10.1016/j.watres.2018.09.056.
[45] Y.-W. Chen, J.-F. Chen, C.-H. Lin, C.-H. Hou, Integrating a supercapacitor with capacitive deionization for direct energy recovery from the desalination of brackish water, Appl. Energy 252 (January) (2019) 113417, https://doi.org/10.1016/j.apenergy.2019.113417.
[46] P. Długołecki, A. Van Der Wal, Energy recovery in membrane capacitive deionization, Environ. Sci. Technol. 47 (9) (2013) 4904–4910, https://doi.org/10.1021/es3053202.
[47] A. Rommerskirchen, C.J. Linnartz, D. Müller, L.K. Willenberg, M. Wessling, Energy recovery and process design in continuous flow-electrode capacitive deionization processes, ACS Sustain. Chem. Eng. 6 (10) (2018) 13007–13015, https://doi.org/10.1021/acssuschemeng.8b02466.
[48] W. Li, X. Lv, Y. Deng, J. Liu, X. He, A review of non-isolated high step-up DC/DC converters in renewable energy applications, Conf. Proc - IEEE Appl. Power Electron Conf. Expo - APEC 2 (2009) 364–369, https://doi.org/10.1109/APEC.2009.4802683.
[49] K. Matsui, I. Yamamoto, T. Kishi, M. Hasegawa, H. Mori, F. Ueda, A comparison of various buck-boost converters and their application to PFC, IECON Proc. (Ind. Electron Conf.) 1 (2002) 30–36, https://doi.org/10.1109/IECON.2002.1187477.
[50] I.D. Kim, S.H. Paeng, J.W. Ahn, E.C. Nho, J.S. Ko, New bidirectional ZVS PWM sepic/zeta DC-DC converter, IEEE Int. Symp. Ind. Electron. (3) (2007) 555–560, https://doi.org/10.1109/ISIE.2007.4374656.
[51] S. Mekhilef, R. Saidur, A. Safari, A review on solar energy use in industries, Renew. Sustain. Energy Rev. 15 (4) (2011) 1777–1790, https://doi.org/10.1016/j.rser.2010.12.018.
[52] S.A. Hawks, A. Ramachandran, S. Porada, et al., Performance metrics for the objective assessment of capacitive deionization systems, Water Res. 152 (2019) 126–137, https://doi.org/10.1016/j.watres.2018.10.074.
[53] T. Kim, J.E. Dykstra, S. Porada, A. van der Wal, J. Yoon, P.M. Biesheuvel, Enhanced charge efficiency and reduced energy use in capacitive deionization by increasing the discharge voltage, J. Colloid Interface Sci. 446 (2015) 317–326, https://doi.org/10.1016/j.jcis.2014.08.041.
[54] A. Ramachandran, A. Hemmatifar, S.A. Hawks, M. Stadermann, J.G. Santiago, Self similarities in desalination dynamics and performance using capacitive deionization, Water Res. 140 (2018) 323–334, https://doi.org/10.1016/j.watres.2018.04.042.